



Cite this: DOI: 10.1039/d6fb00034g

# Films from bio-based aliphatic/aromatic poly(trimethylene furanoate/sebacate) random copolymers for smart sustainable food packaging: gas permeability properties under different conditions of use and after contact with food simulant fluids

Valentina Siracusa,<sup>ID</sup>\*<sup>a</sup> Giulia Guidotti,<sup>ID</sup>\*<sup>b</sup> Anna Szymczyk,<sup>ID</sup><sup>c</sup> Agata Zubkiewicz<sup>e</sup> and Nadia Lotti<sup>ID</sup><sup>b,d</sup>

Films from bio-based poly(trimethylene 2,5-furandicarboxylate-co-trimethylene sebacate) (PTFcoPTSeb) random copolymers were deeply characterized from the gas permeability point of view in order to evaluate their possible use for food packaging under different conditions of temperature and humidity. From previous studies of the same authors, such films appeared very promising, showing smart gas permeability properties under standard testing conditions (23 °C) to oxygen (O<sub>2</sub>) and carbon dioxide (CO<sub>2</sub>), the primary gases of interest in food packaging applications. In detail, in the present paper, the influence of temperature on gas permeability was assessed at 5 °C, 15 °C, and 38 °C, with the lowest value mimicking refrigeration conditions and the highest value the temperature of tropical countries. Furthermore, the films were subjected to food simulant exposure, specifically 10% v/v ethanol (to mimic fatty foods) and 3% w/v acetic acid (to represent aqueous foods). Last but not least, to evaluate the impact of humidity, the samples were conditioned in two distinct relative humidity (RH) environments: a temperate climate (23 °C, 85% RH, using saturated KCl) and a tropical climate (38 °C, 90% RH, using saturated KNO<sub>3</sub>). The films after contact with food simulants were analyzed with respect to gas permeability performance, thermal behavior, mechanical properties, and optical characteristics (including color and transparency). Comparative analysis with untreated films revealed a strong correlation between the copolymer composition, treatment conditions, and resultant performance. While each treatment exhibited a distinct influence depending on the chemical structure of the material, all copolymers demonstrated excellent permeability properties against O<sub>2</sub> and CO<sub>2</sub>. Among the investigated materials, the copolymer containing 15 mol% PTSeb exhibited the most balanced performance under dry conditions, while showing limitations under high humidity conditions. Thermal analysis confirmed the chemical stability of the copolymer films post-treatment, and mechanical testing indicated the preservation of their structural integrity. The films remained transparent, exhibiting a slight yellowing, which intensified marginally according to the various treatments.

Received 6th February 2026  
Accepted 2nd April 2026

DOI: 10.1039/d6fb00034g

rsc.li/susfoodtech

## Sustainability spotlight

This study highlights the strong sustainability potential of bio-based poly(trimethylene 2,5-furandicarboxylate-co-trimethylene sebacate) (PTFcoPTSeb) copolymer films, as innovative materials for next-generation food packaging. Derived from renewable resources, these copolymers were thoroughly evaluated under realistic environmental conditions, including variable temperatures, humidity levels, and exposure to food simulants, to assess their performance throughout the product's entire life cycle. Combining renewable raw materials, excellent functional performance and high stability under stress conditions, these bio-based films represent a promising and environmentally responsible alternative to traditional fossil-based plastics in food packaging applications. Their adoption has the potential to reduce the carbon footprint, improve resource efficiency, and support a circular materials economy.

<sup>a</sup>Department of Chemical Science, University of Catania, Viale A. Doria 6, 95125 Catania (CT), Italy. E-mail: vsiracus AT dmfc.unicat.it

<sup>b</sup>Department of Civil, Chemical, Environmental, and Materials Engineering, University of Bologna, Via Terracini 28, 40131 Bologna, Italy. E-mail: giulia.guidotti9 AT unibo.it

<sup>c</sup>Department of Mechanical Engineering and Mechatronics, West Pomeranian University of Technology, Al. Piastów 19, PL 70-310 Szczecin, Poland

<sup>d</sup>Interdepartmental Center for Agro-Food Research, CIRI-AGRO, University of Bologna, Bologna, Italy

<sup>e</sup>Institute of Mathematics, Physics and Chemistry, Maritime University of Szczecin, Waly Chrobrego 1, 2, Szczecin 70-500, Poland



# 1 Introduction

According to recent data, over 430 million tons of plastic are produced annually worldwide, a figure that is projected to increase, reaching an estimated 1 billion tons during the 2050–2060 decade.<sup>1,2</sup> Plastics are extensively employed across a wide range of sectors owing to their remarkable versatility, low cost, light weight, ease of processing, chemical and physical stability, and excellent mechanical performance. However, their high durability contributes to environmental persistence: improperly disposed plastic materials can remain in the environment for centuries, thereby contributing significantly to pollution and ecological degradation.<sup>3</sup>

Moreover, the vast majority of plastics currently in use are derived from fossil resources, further exacerbating greenhouse gas emissions and the depletion of non-renewable feedstocks. A substantial portion of these plastics is employed in the food industry, where packaging lifespans are intrinsically short due to the limited shelf life of the products they contain.<sup>4</sup>

Food waste itself is another pressing environmental issue, contributing to resource inefficiency (land and water), unnecessary emissions, and other ecological impacts including acidification and eutrophication. Consequently, mitigating the environmental burden of both food and plastic wastes is a shared concern among scientists, industry stakeholders, and consumers alike. The current focus lies in the development of materials that preserve food safety and integrity while minimizing environmental harm.

Two interrelated strategies are of primary importance: reducing food waste and decreasing the reliance on fossil-derived packaging materials. Effective packaging plays a critical role in extending the shelf life, ensuring food quality, and preventing contamination throughout the food supply chain, thereby directly contributing to food waste reduction.

As a result, significant attention has been directed toward the development of bioplastics for food packaging applications.<sup>5–7</sup> Bioplastics may be wholly or partially derived from renewable sources, including agricultural and food wastes, and may be biodegradable or not, depending on their chemical structure and susceptibility to microbial degradation.<sup>8</sup>

Currently, the production volume of bioplastics remains limited, and only a few bioplastics, such as poly(lactic acid) (PLA), poly(butylene succinate) (PBS) and poly(butylene adipate-*co*-terephthalate) (PBAT), are commercially employed in the food packaging sector.<sup>2,7,9</sup>

However, a major limitation of aliphatic polyesters in general is their poor gas permeability performance, a critical property in food packaging. Indeed, the permeability to gases such as oxygen and carbon dioxide must be tightly controlled to maintain food quality and safety.<sup>10</sup>

In this context, aromatic polyesters, particularly those synthesized from 2,5-furandicarboxylic acid (FDCA)—one of the U.S. Department of Energy's top 12 bio-based building blocks—have emerged as promising alternatives due to their exceptional gas permeability properties.<sup>2,11–15</sup> These materials, fully derived from renewable resources, are being evaluated as potential

replacements for fossil-based plastics like poly(ethylene terephthalate) (PET).<sup>16–18</sup>

Moreover, furan-based polymers can be engineered to be either biodegradable or non-biodegradable, depending on their chemical structure and molecular architecture. By modulating the balance between aromatic and aliphatic moieties (the latter typically derived from glycols or aliphatic diacid co-units), it is also possible to tailor key properties, especially gas permeability.<sup>19–21</sup>

One of the most extensively studied furan-based polymers is poly(trimethylene furanoate) (PTF), representing, together with poly(ethylene furanoate), PEF, the bio-based analogue of PET. PTF exhibits not only favorable thermal and mechanical properties but also significantly improved gas permeability performances—it is 4–5 times less permeable to O<sub>2</sub> and 27 times less permeable to CO<sub>2</sub> than PET.<sup>19</sup>

However, similar to PET, PTF is not inherently biodegradable or compostable. Thus, copolymerization with aliphatic, biodegradable monomers is an approach, which has been widely documented and offers a viable strategy to modulate end-of-life behavior.<sup>22–27</sup>

In a previous study, we investigated random copolymers of PTF and poly(trimethylene sebacate) (PTSeb)—an aliphatic, fully bio-based polyester derived from castor oil and sugars.<sup>21</sup> These materials were evaluated for their chemical, mechanical, gas permeability, and compostability properties under standard conditions.<sup>21,28</sup> Although our previous study focused on the synthesis and intrinsic properties of PTF-*co*-PTSeb copolymers under standard conditions, a comprehensive understanding of their behavior in realistic food packaging environments is still lacking.<sup>21</sup> Recent advances in sustainable polymeric materials have highlighted the importance of tailoring structure–property relationships through molecular design and advanced characterization techniques in order to achieve targeted functional performance.<sup>29–31</sup>

In this work, we aim to fill this gap by systematically studying the gas barrier performance of these materials under conditions that closely simulate real applications, including variable temperature, high relative humidity, and exposure to food simulants mimicking fatty and aqueous foods. This methodology enables us to move from intrinsic material characterization to application-relevant performance assessment.

To our knowledge, no previous study has thoroughly investigated the performance of furan-based bioplastics under different conditions. In this study, we have investigated films obtained from PTF-based copolymers with different proportions of TSeb co-units (5%, 15%, and 25% mol), corresponding to distinct material behaviors in terms of chain mobility, phase structure and gas barrier performance, selected to evaluate how the functional properties change in realistic packaging environments. Sebacic acid was not introduced to improve all properties, but to make the material usable by balancing rigidity, flexibility and environmental performance. This strategy allows us to move from intrinsic material characterization to application-relevant performance assessment.

Future studies will include evaluation of water vapor permeability to provide a more comprehensive assessment of



the suitability of these materials for food packaging applications.

## 2 Materials and methods

### 2.1 Materials

Dimethyl-2,5-furandicarboxylate (DMF) (99.5%) was supplied by Matrix Fine Chemicals GmbH (Switzerland); dimethyl sebacate (DMS) (99%) and tetrabutyl orthotitanate (TBT) (97%) were purchased from Sigma-Aldrich Co; pentaerythritol tetrakis[3-(3,5-di-*tert*-butyl-hydroxyphenyl)propionate (Irganox 1010), used as an antioxidant, is from BASF Corporation; bio-based 1,3-propanediol (PDO) (98%) (Susterra®) was kindly gifted by DuPont Tate & Lyle Bio Products Company, LLC (Loudon, TN, USA).

All chemicals were used without further purification except for PDO, which was purified by distillation before use.

All characterization experiments were performed on three independently prepared film samples for each composition, and the reported values represent the average of these measurements.

### 2.2 Polymers

Poly(trimethylene 2,5-furanoate-*co*-trimethylene sebacate) (PTFcoPTSeb) copolymers were synthesized by two step melt polycondensation, starting from the proper relative amounts of DMF and DMS, PDO in a molar excess of 220% and TBT (0.125 wt% of the amount of the diesters) as the catalyst, in a stirred steel reactor, according to the procedure already reported in the literature.<sup>21</sup>

The chemical structure of the synthesized copolymers is shown in Fig. 1.

In the present work, these materials were processed into films by thermal compression (Carver C12 laboratory press), molding the polymers between two Teflon plates at temperatures approximately 30 °C above their melting point. After melting, a pressure of 2 ton per m<sup>2</sup> was applied and then the films were cooled down to room temperature inside the press.

These compositions were chosen as they are representative of several structural regimes identified in previous studies.<sup>21</sup> Fig. 2 provides a conceptual representation of the relationship between copolymer composition and material behavior, highlighting the rationale behind the selection of the analyzed compositions.

### 2.3 Thickness determination

The film thickness, expressed in microns, was determined using a Sample Thickness Tester DM-G (Brugger Feinmechanik GmbH, Munich, Germany), consisting of a digital dial indicator with a resolution of 0.001 microns. The thickness values used for measurements represent the mean value of three experimental tests performed at different points (10 points) on the surface of the polymer film at room temperature.<sup>32</sup> Films with a thickness of 100–150 microns were obtained.

Film thickness was measured for each sample and explicitly included in the permeability calculation, which is normalized to thickness according to the standard definition, thus accounting for any variability in film thickness.

### 2.4 Gas permeability measurements

The determination of the gas permeability behavior was performed using a manometric method, with a Permeance testing device, type GDP-C (Brugger Feinmechanik GmbH, Munich, Germany), according to ASTM 1434-82 (Standard test Method for Determining Gas Permeability Characteristics of Plastic Film and Sheeting), DIN 53 536 (gas permeability determination) in compliance with ISO/DIS 15 105-1 (plastic film and sheeting-determination of gas transport rate: – part I: differential pressure method, 2007), and according to the Gas Permeability Testing Manual.<sup>33</sup> The instrument is equipped with two chambers, an upper and a lower one, between which the polymer film is placed (with an analysis area of 78.4 cm<sup>2</sup>). At the start of each measurement, the upper chamber is filled with the test gas (upper pressure equal to 1 atm and a gas flow rate of 100 cm<sup>3</sup> min<sup>-1</sup>), while the lower chamber is brought under vacuum using an external pump connected to the instrument. The

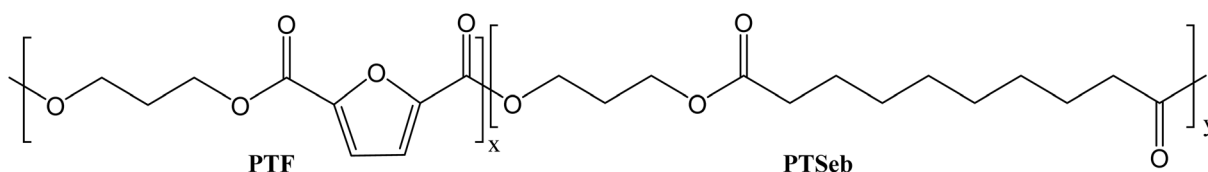


Fig. 1 Chemical structure of (PTFcoPTSeb) copolymers.

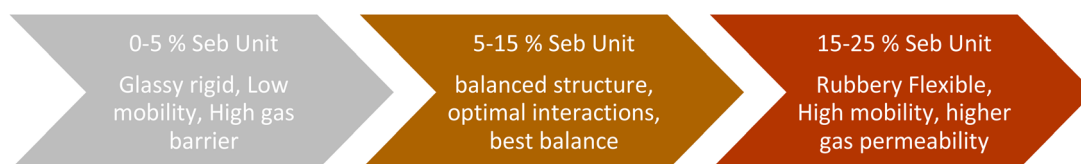


Fig. 2 PTSeb content (mol%).



analysis temperature chosen for the test is regulated using an external thermostat type HAAKE-Circulator DC10-K15 (Thermoscientific, Selangor Darul Ehnsan, Malaysia), also connected to the instrument. By measuring the pressure variation of the gas between the upper and lower chambers, as a function of time and the volume of the device, the Gas Transmission Rate (GTR) values, expressed by the instrument in  $\text{cm}^3 \text{m}^{-2}$  per d per bar of the polymer film are recorded, calculated and logged by the software. The GTR values obtained were normalized for the film thickness and the pressure was expressed in atmospheres in order to determine the permeability expressed in  $\text{cm}^3 \text{cm}^{-2}$  per d per atm. This unit was chosen to compare our results with those reported in the literature. The values reported are the average of three measurements  $\pm$  standard deviation.

The transport phenomenon background followed is that described in the literature.<sup>34,35</sup> The pressure was given by the instrument in bar units. In order to obtain the data values in kPa (SI units) the following correction factor 1 bar = 10 kPa was used, according to NIST special publication 811.<sup>36</sup>

The instrument was calibrated in accordance with the manufacturer's procedure (GDP-C Brugger Feinmechanik GmbH, Munich, Germany). Calibration was performed at 23 °C using a 50 micron steel blocking film with air as the test gas (sample area of 78.4  $\text{cm}^2$ ), and at 23 °C with a 100 micron polyethylene terephthalate (PET) reference film under an  $\text{O}_2$  gas flow (sample area of 78.4  $\text{cm}^2$ ).

## 2.5 Relative humidity solution

According to the procedure described in the Gas Permeability Testing Manual, the different relative humidity (RH) environments were obtained by using different saturated saline solutions.<sup>33</sup> In particular, a round filter paper (Filter Paper MN 85/70 BF 70 mm diameter, Macherey-Nagel, GmbH & Co. KG, Germany) was humidified with the desired saturated saline solution and was fixed with a suitable plastic perforated ring, screwed to the upper permeation chamber, in order to humidify the gas flow.<sup>33</sup> Two different relative humidity (RH) environments were used, obtained with two saturated salt solutions (standard atmosphere, 23 °C, and 85% RH, with saturated KCl solution; tropical climate, 38 °C, and 90% RH, with saturated  $\text{KNO}_3$  solution). The relative humidity values for the salt solutions were obtained from DIN 53 122 part 2. Method C was used, with the gas flow blocked in the upper chamber during evacuation, where the film sample under test is located.<sup>33</sup> The test gas is then automatically humidified inside the permeation cell. The upper chamber of the test sample, filled with the humidified gas, is subjected to normal ambient pressure, while the lower chamber is evacuated and brought under atmospheric pressure.<sup>33</sup> The GTR values obtained were normalized for the film thickness and reported as the average of three measurements  $\pm$  standard deviation.

## 2.6 Simulant liquids

Tests with food contact simulant liquids were performed in accordance with the EU Regulation No. 10/2011 on plastic materials and articles intended to come into contact with

food.<sup>37</sup> Two solutions were used as food simulants: (1) simulant A, ethanol 10% (v/v), 10 days, and 40 °C; (2) simulant B, acetic acid 3% (v/v), 10 days, and 40 °C. Each film sample of 3 cm  $\times$  3 cm was fully immersed in 200 mL of the simulant put into closed glass jars. The jars were then placed in an incubator (Stuart SI500), at the selected temperature for the time period defined. After the analysis time had elapsed, the samples were removed from the jar, washed with distilled water twice and dried with absorbent paper. Before analysis, the films were stored at room temperature, under dry environmental conditions for at least two weeks. The samples were tested in triplicate. The EU Regulation No. 10/2011 considers different degrees of stress treatments (mainly varying contact times with simulant food liquids). In this work, the conditions that mimic the worst-case scenario were applied.

## 2.7 Color evaluation

The color of the film samples was measured using a HunterLab ColorFlex EZ 45/0° color spectrophotometer (Reston, VA, USA) with a D65 illuminant and 10° observer according to ASTM E308.<sup>38</sup> Measurements were recorded using the CIE Lab scale. The instrument was calibrated with a black and white tile before the measurements. The results were expressed as  $L^*$  (lightness),  $a^*$  (red/green), and  $b^*$  (yellow/blue) parameters. The total color difference ( $\Delta E$ ) was calculated using the following equation:

$$\Delta E = [(\Delta L)^2 + (\Delta a)^2 + (\Delta b)^2]^{0.5}$$

where  $\Delta L$ ,  $\Delta a$ , and  $\Delta b$  are the differentials between a sample color parameter ( $L^*$ ,  $a^*$ , and  $b^*$ ) and the color parameter of a standard white plate used as the film background ( $L' = 66.39$ ,  $a' = -0.74$ , and  $b' = 1.25$ ).

Chromaticity ( $C^*$ ) and hue angle ( $h_{\text{ab}}$ ) were calculated as previously reported in the literature, according to the following equations:<sup>39–43</sup>

$$C^* = [(a^*)^2 + (b^*)^2]^{0.5}$$

$$h_{\text{ab}} = [\arctan (b^*/a^*)/2\pi] 360$$

Measurements were recorded in triplicate at random positions over the film surface, and the results are reported as the average values of these three experiments.

## 2.8 Thermal analysis

Differential scanning calorimetry (DSC) measurements on the samples after contact with food simulants were performed using a PerkinElmer (Waltham, MA, USA) DSC6 under a pure  $\text{N}_2$  flow (20  $\text{mL min}^{-1}$ ). The thermal heating scan was performed from  $-60$  to  $200$  °C at a rate of  $20$  °C  $\text{min}^{-1}$  on each film sample (about 10 mg). The glass transition temperature ( $T_g$ ) was determined as the midpoint of the glass-to-rubber transition step, while the associated specific heat increment ( $\Delta C_p$ ) was calculated as the height of the baseline deviation related to the glass-to-rubber transition. The melting temperature ( $T_m$ ) and the cold crystallization temperature ( $T_{cc}$ ) were calculated as the



maximum/minimum of the endothermic/exothermic phenomena in the DSC curves, respectively, while the corresponding enthalpy of melting ( $\Delta H_m$ ) and enthalpy of crystallization ( $\Delta H_{cc}$ ) were obtained from the areas of the endothermic and exothermic phenomena, respectively.

## 2.9 Mechanical analysis

Tensile mechanical tests were performed at room temperature on film specimens (50 × 5 mm and gauge length of 20 mm) after contact with food simulants by means of an INSTRON 5966 testing machine (Norwood, MA, USA) equipped with a 1 kN transducer-coupled load cell and Bluehill software. A constant crosshead speed of 10 mm min<sup>-1</sup> was applied. The Young's modulus ( $E$ ), stress at break ( $\sigma_B$ ) and elongation at break ( $\epsilon_B$ ) were calculated from the obtained stress-strain curves. The reported results are the mean values ± standard deviation of seven measurements.

## 2.10 Statistical analysis

All experimental data including gas permeability, mechanical properties and color parameters ( $L^*$ ,  $a^*$ ,  $b^*$ ) were statistically analyzed by using an analysis of variance (ANOVA) followed by Tukey's HSD *post hoc* test to compare the means at the level of confidence of 95% ( $p < 0.05$ ). The analysis was performed using the software STATISTICA 6.0 (Statsoft Inc., Tulsa, UK).

# 3 Results and discussion

## 3.1 General behavior of PTF and its copolymers

The poly(trimethylene furanoate) (PTF) homopolymer and three PTF-based aromatic/aliphatic copolymers, named PTFcoPTSeb, with aliphatic trimethylene sebacate co-unit content ranging from 5 to 25 mol% were successfully synthesized by the well-known two stage melt polycondensation procedure, without the use of chemical solvents. The results of molecular characterization are collected in Table 1 and described in detail in a previous study.<sup>21</sup> In brief, the actual composition, calculated through <sup>1</sup>H-NMR, is in line with the feed one, and the degree of randomness of the copolymers ( $R$ ) is close to 1, as expected, indicating a random distribution of the sequences. Moreover, according to GPC measurements, all the materials have high number average molecular weights ( $M_n$ ) and polydispersity indices ( $D$ ) close to 2, typical for polycondensation processes, allowing the exclusion of an effect of these parameters on the properties described in the following section.

## 3.2 Gas permeability properties

The permeability values are expressed as cm<sup>3</sup> (STP) cm m<sup>-2</sup> per d per atm. This value was normalized to the thickness of the sample, measured before each permeability test. To convert this unit of measurement into others reported in the literature, the conversion factors reported by Robertson could be used.<sup>43</sup> The theoretical models used, the mechanism of the permeation process and the permeability coefficients have been previously described in the literature.<sup>32,35,44</sup>

Carbon dioxide and oxygen were chosen as test gases, being the main gases used in the food packaging field. They can permeate through the packaging wall, continuously affecting the shelf life of food as well as its safety and quality.

Temperature, film thickness, chemical structure of the polymer, environmental humidity and type of food are all parameters that can strongly influence the final performance of the considered food packaging, compromising its proper functioning.

Gas permeability refers to the ability of a polymer film or membrane, to allow gases to pass through it. It is a measure of how easily gas molecules can diffuse and dissolve within the material. Permeability depends mainly on diffusivity ( $D$ ), which describes how easily the gas molecules move through the polymer matrix, and solubility ( $S$ ), which describes how much gas can dissolve in the material.<sup>43</sup> The overall permeability coefficient ( $P$ ) is given by the product  $P = D \times S$ , meaning that a material with high diffusivity or high solubility will have greater permeability to that gas.<sup>43</sup> It should be noted that the permeability measurements were performed using a pressure-sensing permeation device (Brugger GDP-C), in which gas transport is evaluated based on the pressure variation across the film. Under these conditions, the permeation curves obtained for the analyzed samples do not exhibit a well-defined time-lag region, which is necessary for the reliable determination of diffusion coefficients. The shape of the transient response depends strongly on the intrinsic characteristics of the films and, in this specific case, does not allow for accurate separation of diffusion and solubility contributions.

Therefore, the analysis is limited to permeability, which represents the most robust and experimentally accessible parameter under the conditions used.<sup>43</sup>

The film samples were analyzed at 23 °C (standard conditions) and at 8, 15 and 38 °C, in order to study the temperature-permeability dependence in a dry environment. Then, two different ambient moisture environments, simulating the standard atmosphere (23 °C and 85% RH) and the tropical

**Table 1** Molecular characterization data of PTFcoPTSeb copolymers

Sample	PTSeb feed (mol%)	PTSeb actual (mol%)	$R$ (—)	$M_n$ (g mol <sup>-1</sup> )	$M_w$ (g mol <sup>-1</sup> )	$D$ (—)	Phase behavior
PTF	0	0	—	34 460	69 610	2.02	Glassy amorphous
PTF5PTSeb	5	5.26	0.98	42 810	100 630	2.35	Glassy amorphous
PTF15PTSeb	15	14.39	1.09	43 040	105 160	2.44	Semirubbery amorphous
PTF25PTSeb	25	24.28	1.10	51 010	139 100	2.72	Rubbery semicrystalline



**Table 2** O<sub>2</sub> and CO<sub>2</sub> permeability values (cm<sup>3</sup> (STP) cm m<sup>-2</sup> per d per atm) at different temperatures (8, 15, 23 and 38 °C), 23 °C/85% RH and 38 °C/90% RH, together with extrapolated E<sub>a</sub> values

Sample/ temperature	8 °C	15 °C	23 °C <sup>a</sup>	23 °C, 85% RH	38 °C	38 °C, 90% RH	E <sub>a</sub> (kJ mol <sup>-1</sup> )
<b>O<sub>2</sub></b>							
PTF	0.0307 ± 0.0080 <sup>a</sup>	0.0340 ± 0.0060 <sup>a</sup>	<b>0.0800 ± 0.0100<sup>b</sup></b>	0.1018 ± 0.0190 <sup>b</sup>	0.1000 ± 0.0200 <sup>b</sup>	0.1599 ± 0.0200 <sup>ab</sup>	31.49
PTF5PTSeb	0.0645 ± 0.0070 <sup>ab</sup>	0.1265 ± 0.0100 <sup>b</sup>	<b>0.1295 ± 0.0200<sup>b</sup></b>	0.1380 ± 0.0200 <sup>b</sup>	0.4681 ± 0.0200 <sup>c</sup>	0.7977 ± 0.0200 <sup>b</sup>	45.34
PTF15PTSeb	0.1178 ± 0.0110 <sup>bc</sup>	0.1843 ± 0.0200 <sup>b</sup>	<b>0.0022 ± 0.0010<sup>a</sup></b>	0.0712 ± 0.0080 <sup>a</sup>	0.0029 ± 0.0010 <sup>a</sup>	2.1428 ± 0.2000 <sup>c</sup>	-108.79
PTF25PTSeb	0.2751 ± 0.0390 <sup>c</sup>	0.2855 ± 0.0200 <sup>c</sup>	<b>0.8212 ± 0.0200<sup>c</sup></b>	0.2235 ± 0.0200 <sup>c</sup>	2.0172 ± 0.1000 <sup>d</sup>	4.5316 ± 0.2000 <sup>d</sup>	52.41
<b>CO<sub>2</sub></b>							
PTF	0.0184 ± 0.0070 <sup>a</sup>	0.0229 ± 0.0060 <sup>b</sup>	<b>0.0500 ± 0.0100<sup>b</sup></b>	0.1271 ± 0.009 <sup>b</sup>	0.0538 ± 0.0050 <sup>b</sup>	0.0556 ± 0.0060 <sup>a</sup>	28.01
PTF5PTSeb	0.0360 ± 0.0080 <sup>a</sup>	0.0151 ± 0.0080 <sup>ab</sup>	<b>0.1457 ± 0.0200<sup>c</sup></b>	0.0802 ± 0.0020 <sup>a</sup>	0.1699 ± 0.0080 <sup>c</sup>	0.0108 ± 0.0040 <sup>b</sup>	50.39
PTF15PTSeb	0.0236 ± 0.0060 <sup>a</sup>	0.0032 ± 0.0010 <sup>a</sup>	<b>0.0026 ± 0.0010<sup>a</sup></b>	0.3840 ± 0.0030 <sup>c</sup>	0.0045 ± 0.0020 <sup>a</sup>	2.9762 ± 0.2000 <sup>c</sup>	-31.54
PTF25PTSeb	0.3453 ± 0.0290 <sup>c</sup>	0.355 ± 0.0220 <sup>c</sup>	<b>2.3000 ± 0.1000<sup>d</sup></b>	1.9846 ± 0.110 <sup>d</sup>	7.1228 ± 0.3000 <sup>d</sup>	11.3159 ± 0.7000 <sup>d</sup>	80.70

<sup>a</sup> From the literature.<sup>21</sup> Different lowercase letters within the same column indicate statistically significant differences between samples ( $p < 0.05$ ), based on ANOVA followed by Tukey's *post hoc* test.

atmosphere (38 °C and 90% RH), were evaluated and the permeability of the films was tested under these conditions. Finally, the permeability behavior was also measured after food simulant contact (water solution containing ethanol 10% v/v and water solution of acetic acid 3% w/v), simulating foods containing a high amount of fats and foods rich in water, respectively.

The values of O<sub>2</sub> and CO<sub>2</sub> permeability at different temperatures (8, 15, 23 and 38 °C) and humidity (85 and 90% RH), together with the calculated values of activation energy are collected in Table 2 and plotted in Fig. 3 and 4, respectively.

Both PTF and the copolymers under consideration are characterized by superior oxygen and carbon dioxide permeability properties at 23 °C, RH = 0% compared to polyolefins (LDPE:  $P_{O_2} = 30$ ,  $P_{CO_2} = 140$ ; HDPE:  $P_{O_2} = 15$ ,  $P_{CO_2} = 20$ ; PP:  $P_{O_2} = 10$ ,  $P_{CO_2} = 65$ , all expressed in cm<sup>3</sup> (STP) cm m<sup>-2</sup> per d per atm) and PET ( $P_{O_2} = 0.36$ ,  $P_{CO_2} = 1.37$  cm<sup>3</sup> (STP) cm m<sup>-2</sup> per d per atm), currently widely used for food packaging films.<sup>43,45</sup>

PTF and PTF5PTSeb present low and comparable GTR values, due to their glassy state at room temperature, which means low chain mobility and consequently low free volume through which gases can pass. The PTF15PTSeb sample is the best performing, despite its amorphous nature and a  $T_g$  around room temperature, *i.e.* test temperature. The outstanding behavior is due to the ability at this temperature of macromolecular chains to rearrange and interact with each other (through interchain pseudo-hydrogen bonding and  $\pi$ - $\pi$  interactions), maximizing the physical connections between chains, which make the amorphous phase very dense and therefore more able to hinder the passage of gas.<sup>21</sup> Furthermore, the absence of a crystalline phase in the polymer matrix determines the minimization of interphase disclinations, the latter being possible preferential channels for the passage of gases. The PTF25PTSeb sample, instead, shows the highest permeability values, due to the presence of crystallites and hence disclinations between the crystalline and amorphous phases, which create preferential channels for the passage of gases.<sup>21</sup>

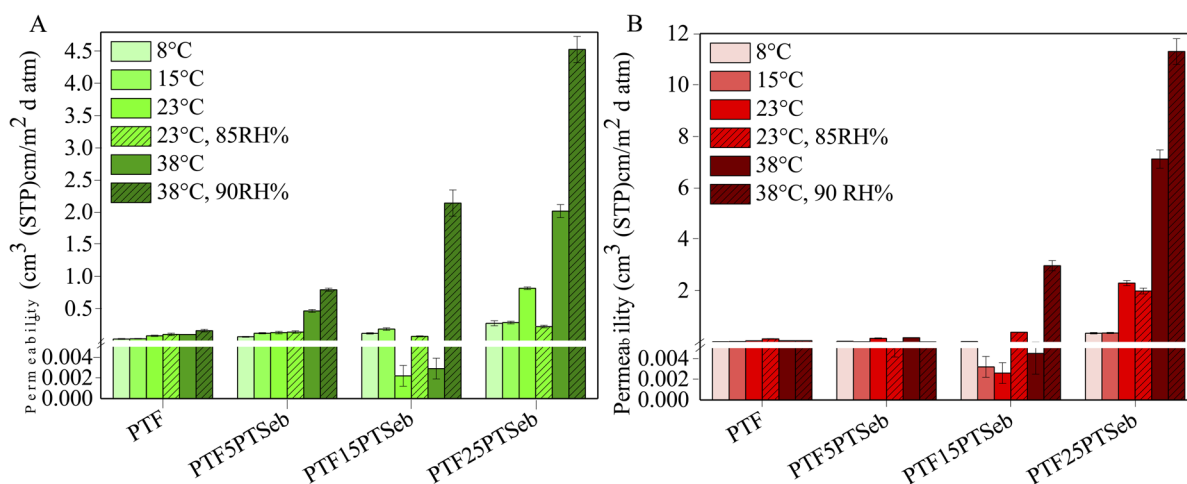


**Fig. 3** Effect of temperature and relative humidity (RH) on permeability: (A) for O<sub>2</sub> and (B) for CO<sub>2</sub>.



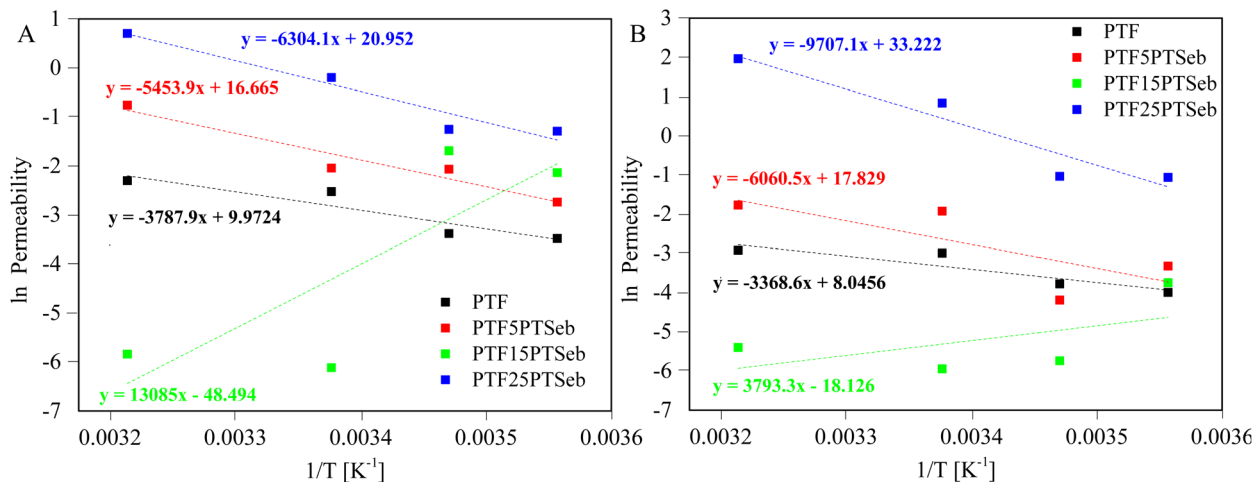


Fig. 4 (A) ln(O<sub>2</sub>) and (B) ln(CO<sub>2</sub>) permeability as a function of 1/T.

This interpretation is consistent with previous studies on furan-based polyesters, including our previous work, where spectroscopic and thermal analyses suggested the presence of intermolecular interactions that contribute to improved barrier properties.<sup>21,42,44,47</sup> The relationship among molecular structure, intermolecular interactions, and transport properties observed in this work is consistent with broader trends reported in advanced polymer systems, where the role of chain organization and environmental conditions has been widely discussed.<sup>48,49</sup>

Temperature is one of the most important parameters when a material is used as food packaging, because it significantly affects the respiration rate of food. To understand how temperature affects the permeability of materials, permeability measurements have been performed at different temperatures. In particular, a temperature range from 8 to 38 °C was taken into consideration, to mimic different possible scenarios, such as storage (lower temperatures, 8 and 15 °C) and handling (higher temperatures, 23 and 38 °C). In general, gas permeability increases with increasing temperature, since the increased kinetic energy of the gas molecules and the greater mobility of the polymer chains facilitate gas diffusion. Gas molecules move faster and with more energy as the temperature increases, making it easier for them to penetrate the material. Increasing the temperature also increases the mobility of the polymer chains, creating more space between them and allowing more gas molecules to pass through the material (free volume increases). Such an expected trend with temperature is found for all the samples under investigation apart from PTF15PTSeb, which exhibited better performance at 23 °C to both gases. The exceptional behavior can be attributed to the ability of macromolecular chains, at temperatures close to the  $T_g$ , to rearrange and establish intermolecular interactions, which can increase the density of the amorphous phase and hinder gas diffusion. This interpretation is consistent with previous results reported in our previous work, where FTIR analysis suggested the presence of intermolecular interactions and thermal analysis highlighted a dense amorphous structure associated with improved barrier properties.<sup>21</sup>

To describe the dependence of permeability on temperature, an Arrhenius-type model was considered, through a mathematical correlation between permeability and temperature.<sup>32,34,42,46,47</sup> The equation shows that permeability increases exponentially as temperature increases, according to the equation  $P = P_0 e^{-E_a/RT}$ , where  $P_0$  is the pre-exponential factor,  $E_a$  is the activation energy for permeation,  $R$  is the gas constant and  $T$  is the absolute temperature. According to exponential dependence, even a small increase in temperature can have a significant impact on permeability. The activation energy term represents the energy required for gas molecules to pass through the material. A higher  $E_a$  value means that the permeability depends more strongly on temperature and consequently the process requires more thermal energy for gas molecules to move through the materials. Moreover,  $E_a$  could have a positive or a negative value: when  $E_a$  is positive, which is the most common case, permeability increases with temperature, because as temperature increases polymer chains gain mobility and the free volume inside the material increases. Therefore, gas molecules could diffuse more easily through the polymer matrix, and, consequently, diffusion  $D$  dominates the permeation process.<sup>29,43,50–52</sup> This behavior is typically observed in commercial glassy polymers (like PET or nylon) or in general, below the glass transition temperature ( $T_g$ ), where chain mobility is limited and the temperature has a strong effect. However, in less common cases, activation energy is negative, meaning that the permeability decreases as temperature increases, due to a decrease in gas solubility, even if diffusion becomes faster, and to a predominant effect of solubility over diffusivity. Consequently, the overall permeability can decrease.<sup>53–57</sup>

The activation energy for the gas transmission rate ( $E_a$ ) was calculated from the slope ( $-E_a/R$ ) of the straight line obtained by plotting ln(GTR) as a function of 1/T, with  $R$  (universal gas constant) equal to 8.314 J mol<sup>-1</sup> K<sup>-1</sup> (Fig. 4). In all cases, a good linear trend was observed, except for the PTF15PTSeb sample, for which the values are more scattered. As expected, all the lines have a negative slope (that means a positive value of



activation energy), except for the copolymer containing 15 mol% of the trimethyl sebacate co-unit.

According to the literature, the activation energies for the gas migration process through a plastic film range from 12 to 63 kJ mol<sup>-1</sup>.<sup>32</sup> As to the materials under study, all the films are characterized by  $E_a$  values included in this range.<sup>50,58,59</sup> Again, PTF15PTSeb, the best performing sample at 23 °C 0% RH, is an exception.

As is known from the literature, for furan-based polyesters, humidity can have two opposite effects on permeability: on the one side, water molecules exert a plasticizing effect, which increases the free volume (glass transition temperature decreases) worsening the gas permeability performances; on the other side, H<sub>2</sub>O molecules actively interact with polymer macromolecules enhancing the H-bond bridges, thus further improving gas locking and, consequently, reducing GTR values.<sup>60</sup> Regarding the oxygen gas test, worsening of permeability properties with humidity is observed in all samples, which is more consistent at 38 °C. As to the CO<sub>2</sub> gas test, two different behaviors can be observed according to the amount of the aliphatic co-unit: in the case of the PTF homopolymer and the copolymer containing the lowest amount of the aliphatic co-unit, the presence of humidity improves the gas permeability performances both at 23 and 38 °C; for the two copolymers richest in the TSeb co-unit, an opposite effect was observed, proving that the plasticizing effect prevails for these two samples. However, it should be noted that the gas permeability performance remains very good and significantly better than that of polyolefins.<sup>21,43</sup>

From an application perspective, these results suggest that PTF-co-PTSeb copolymers may be suitable for food packaging applications involving low-moisture products, where high gas barrier properties are required under relatively dry conditions. The significant increase in gas permeability observed at high relative humidity highlights a limitation for applications involving high-moisture foods or tropical environments. Therefore, the effective use of these materials requires careful consideration of storage conditions and the specific requirements of the packaged foods. To the best of our knowledge, no food contact tests have been performed at this time (Table 3).

Fig. 5 shows GTR values for dry oxygen and carbon dioxide after contact with food simulants for all the samples under investigation, compared with the GTR values of untreated samples. In all cases and for each gas, no appreciable worsening of the gas permeability performances is observed, but only

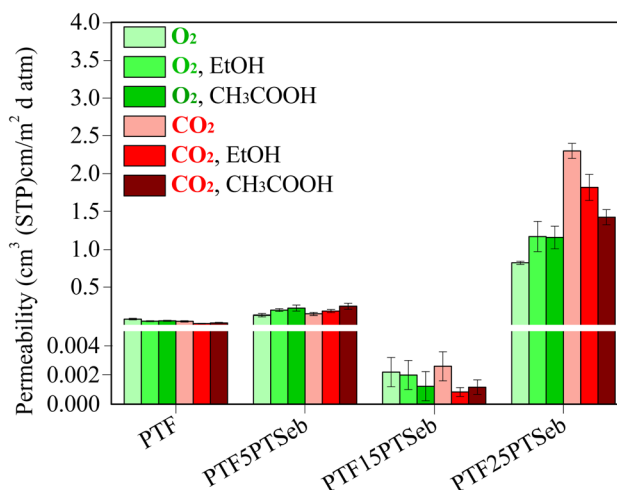


Fig. 5 O<sub>2</sub> and CO<sub>2</sub> permeability after food simulant contact (ethanol 10% v/v; acetic acid 3% w/v).

small variations, which, for some samples, are even indicative of an improvement (CO<sub>2</sub>-TR for PTF15PTSeb and PTF25TSeb after contact with both food simulants). This result is particularly relevant, taking into account that conditions mimicking the worst case have been applied.

In Fig. 6 the perm-selectivity ratio for the samples under investigation at different temperatures and after stress treatment is reported. As known from the literature, the CO<sub>2</sub>-TR/O<sub>2</sub>-TR ratio is related to the different permeability against the two gases, which in turn depends on the types of interaction that the gas molecules have with the material under examination.<sup>43</sup> In particular, these interactions are linked to diffusion, *i.e.* the speed with which the gases move inside the material, and to solubility, *i.e.* the chemical interaction of the gases with the polymer chains. The GTR is related to the gas molecule diameter (size) and to the interaction between gas molecules and the polymer matrix (affinity). Size and affinity determine the permeability value. In general, CO<sub>2</sub>-TR is higher than O<sub>2</sub>-TR, for polymer films, with the CO<sub>2</sub> gas permeation approximately 4–6 times greater than that of O<sub>2</sub> gas.<sup>43</sup> But, as already studied and reported, for furan-based polymers, a different trend was observed.<sup>61</sup> The ratio was approximately equal to 1 at 23 °C using dry gases, meaning that the permeation behavior was equal for both gases. This behavior has been explained, considering the interaction between polarizable carbon dioxide

Table 3 O<sub>2</sub> and CO<sub>2</sub> permeability values (cm<sup>3</sup> (STP) cm m<sup>-2</sup> per d per atm) after food simulant contact (ethanol 10% v/v; acetic acid 3% w/v)

Sample	O <sub>2</sub> permeability (cm <sup>3</sup> (STP) cm m <sup>-2</sup> per d per atm)			CO <sub>2</sub> permeability (cm <sup>3</sup> (STP) cm m <sup>-2</sup> per d per atm)		
	Control <sup>a</sup>	Ethanol 10% v/v	Acetic acid 3% w/v	Control <sup>a</sup>	Ethanol 10% v/v	Acetic acid 3% w/v
PTF	<b>0.0800 ± 0.0100<sup>b</sup></b>	0.0528 ± 0.007 <sup>b</sup>	0.0560 ± 0.0070 <sup>b</sup>	<b>0.0500 ± 0.0100<sup>b</sup></b>	0.0205 ± 0.0050 <sup>b</sup>	0.0300 ± 0.0060 <sup>b</sup>
PTF5PTSeb	<b>0.1295 ± 0.0200<sup>c</sup></b>	0.1955 ± 0.0200 <sup>c</sup>	0.2210 ± 0.0400 <sup>c</sup>	<b>0.1457 ± 0.0200<sup>c</sup></b>	0.1821 ± 0.0200 <sup>c</sup>	0.2460 ± 0.0400 <sup>c</sup>
PTF15PTSeb	<b>0.0022 ± 0.0010<sup>a</sup></b>	0.0020 ± 0.0010 <sup>a</sup>	0.0012 ± 0.0010 <sup>a</sup>	<b>0.0026 ± 0.0010<sup>a</sup></b>	0.0008 ± 0.0003 <sup>a</sup>	0.0012 ± 0.0005 <sup>a</sup>
PTF25PTSeb	<b>0.8212 ± 0.0200<sup>d</sup></b>	1.1700 ± 0.2000 <sup>d</sup>	1.1570 ± 0.1500 <sup>d</sup>	<b>2.3000 ± 0.1000<sup>d</sup></b>	1.8170 ± 0.1700 <sup>d</sup>	1.4260 ± 0.1000 <sup>d</sup>

<sup>a</sup> From the literature.<sup>21</sup> Different lowercase letters within the same column indicate statistically significant differences between samples ( $p < 0.05$ ), based on ANOVA followed by Tukey's *post hoc* test.



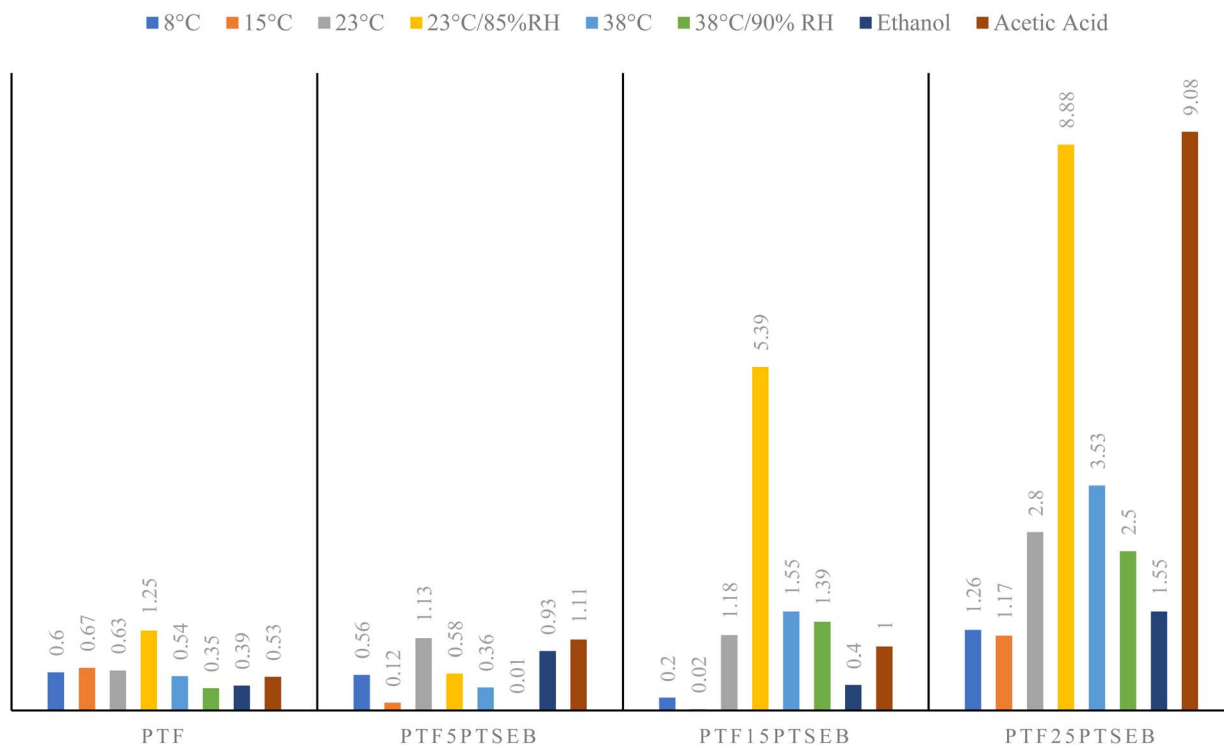


Fig. 6 Perm-selectivity ratios (CO<sub>2</sub>/O<sub>2</sub> permeability ratio) for PTF and PTFCO-PTSeB copolymers at different temperatures and relative humidity and with different simulant liquids.

molecules and the polar groups of polymeric chains (ester group and furan ring). In our investigation, this ratio was always close to 1 or even lower for the PTF homopolymer and the copolymer containing the lowest amount of the TSeB co-unit, remaining constant under humid conditions, at 38 °C and after contact with food simulant fluids. For PTF15PTSeB, the same trend was observed, except at 23 °C and 85% RH. Under these conditions, the perm-selectivity ratio was above 1. Lastly, for the copolymer with the highest amount of the apolar aliphatic co-unit (PTSeB units), the ratio ranged from 1 to 3, becoming even 9 under humid conditions at 23 °C and after contact with acetic acid.

To better highlight the potential fields of application and limitations of the materials studied, Table 4 provides a summary of their performance under different conditions.

It should be noted that the PTF-co-PTSeB copolymers studied are novel materials with no direct commercial equivalents. Therefore, a rigorous comparison with conventional and strictly commercial packaging polymers is not straightforward.

### 3.3 Thermal performances after stress treatments

The phase behaviour of PTF and PTFcoPTSeB copolymers has been evaluated by DSC before and after contact with food simulant solutions. The calorimetric data are reported in Table 5,

Table 4 Possible application scenarios of PTF-co-PTSeB copolymers in food packaging (authors' personal elaboration)

Application scenario	Environmental conditions	Performance of PTF-co-PTSeB	Suitability	Notes/limitations
Dry food packaging (e.g., snacks and cereals)	Low RH and ambient temperature	Excellent gas barrier (O <sub>2</sub> , CO <sub>2</sub> ) and good mechanical integrity	Suitable	Optimal performance under dry conditions
Refrigerated food packaging	Low-moderate RH and low temperature (5–15 °C)	Good barrier properties and reduced permeability due to low temperature	Suitable	Temperature helps limit gas diffusion
Modified atmosphere packaging (MAP)	Controlled humidity and tailored gas composition	Tunable gas permeability depending on copolymer composition	Potentially suitable	Requires controlled RH conditions
Fatty food packaging (after ethanol simulant exposure)	Moderate conditions and contact with fatty simulants	Stable barrier and thermal properties after exposure	Suitable	No significant degradation observed
Aqueous food packaging (after acetic acid exposure)	Moderate RH and contact with aqueous simulants	Good stability and minor variations in properties	Conditionally suitable	Performance depends on the humidity level
High-moisture food packaging	High RH (≥85%)	Significant increase in gas permeability	Not suitable	Strong plasticization effect of water
Tropical environment packaging	High temperature (38 °C) + high RH (90%)	Marked deterioration of barrier performance	Not suitable	Combined effect of T and RH is critical



**Table 5** DSC data from the first scan at 20 °C min<sup>-1</sup> for PTF and PTFcoPTSeb copolymers films, before and after food simulant contact with ethanol 10% v/v and acetic acid 3% w/v

Sample	$T_g$ (°C)	$\Delta C_p$ (J g <sup>-1</sup> °C)	$T_{cc}$ (°C)	$\Delta H_{cc}$ (J g <sup>-1</sup> )	$T_{m1}, T_{m2}$ (°C)	$\Delta H_{m1}, \Delta H_{m2}$ (J g <sup>-1</sup> )
PTF	65 ± 0.11	0.333 ± 0.051	—	—	—	—
PTF-ethanol	51 ± 0.13	0.330 ± 0.099	—	—	165 ± 3.88	37 ± 0.17
PTF-acetic acid	54 ± 0.10	0.273 ± 0.073	132 ± 0.13	18 ± 0.13	165 ± 4.76	18 ± 0.83
PTF5PTSeb	55 ± 0.07	0.398 ± 0.082	—	—	—	—
PTF5PTSeb-ethanol	43 ± 0.08	0.302 ± 0.096	—	—	77 ± 2.54, 157 ± 6.67	7 ± 0.78, 29 ± 0.98
PTF5PTSeb-acetic acid	52 ± 0.11	0.237 ± 0.057	—	—	83 ± 3.88, 156 ± 1.87	7 ± 1.11, 28 ± 1.67
PTF15PTSeb	28 ± 0.19	0.320 ± 0.025	121 ± 0.08	3 ± 0.07	146 ± 2.1	3 ± 0.13
PTF15PTSeb-ethanol	23 ± 0.13	0.323 ± 0.037	—	—	77 ± 1.11, 143 ± 2.01	7 ± 0.34, 25 ± 1.09
PTF15PTSeb-acetic acid	29 ± 0.17	0.222 ± 0.015	—	—	78 ± 1.11, 143 ± 3.65	6 ± 1.10, 26 ± 2.16
PTF25PTSeb	8 ± 0.03	0.147 ± 0.022	—	—	60 ± 2.09, 112 ± 3.11	7 ± 0.78, 23 ± 1.45
PTF25PTSeb-ethanol	3 ± 0.02	0.222 ± 0.013	—	—	74 ± 4.07, 113 ± 1.13	8 ± 0.81, 20 ± 3.07
PTF25PTSeb-acetic acid	6 ± 0.08	0.276 ± 0.054	—	74 ± 0.31, 113 ± 0.87	8 ± 1.13, 21 ± 1.21	—

while the relative traces are shown in Fig. 7. The phase behavior of the molded films was first evaluated, confirming the glassy and amorphous nature of PTF at room temperature ( $T_g = 65$  °C), as a result of its low crystallization ability.<sup>21</sup> Regarding the PTFcoPTSeb copolymers, it was observed that their chain flexibility increases with increasing the amount of the aliphatic PTSeb co-unit, as confirmed by the progressive decrease in  $T_g$  values, from 55 °C for PTF5PTSeb to 28 and 8 °C for PTF15PTSeb and PTF25PTSeb, respectively. Moreover, the copolymers show different crystallization capabilities. In detail, the DSC profile of PTF5PTSeb shows only the glass-to-rubber transition, while in the DSC profile of PTF15PTSeb a slight exothermic crystallization peak appeared, followed by a melting one of the same intensity ( $\Delta H_{cc} = \Delta H_m$ ). Therefore, also this sample can be considered as amorphous. Lastly, for the PTF25PTSeb sample, characterized by a  $T_g$  below room temperature, the macromolecular chains are in a mobile state and consequently can rearrange into an ordered crystalline

structure. As to the position of the melting peak, it can be confirmed that the presence of aliphatic PTSeb units determined a progressive decrease in  $T_m$  values, as a result of copolymerization.<sup>21</sup>

As can be seen from the recorded data (Table 4), the thermal behavior of the samples changes after contact with the simulant liquids. As to PTF, the  $T_g$  values of the treated samples decrease, by about 14 °C after contact with ethanol solution and by about 11 °C upon contact with acetic acid solution, due to the plasticizing effect of these food simulant liquids.<sup>62–64</sup> Moreover, the DSC trace of PTF after contact with acetic acid, shows an exothermic crystallization peak followed by a melting one of the same intensity, meaning that this sample is still amorphous, while after contact with ethanol the sample developed a not negligible percentage of crystallinity. A possible reason for this different behavior can be found in a slight hydrolysis that occurred in the sample in the presence of ethanol, which, in turn, is responsible for the formation of shorter polymeric chains that are more able to crystallize.<sup>65,66</sup> This is reasonable, considering that alcohol assisted alkaline hydrolysis has been documented as an effective route for degradation of aromatic PET fabrics under mild conditions.<sup>67</sup>

For the sample containing 5% of the TSeb co-unit, a notable increase in crystallinity was noted, practically the same for both simulant liquids compared to the non-treated sample. This behavior could be explained, considering that the experiments were carried out at 40 °C, a temperature which is close to the  $T_g$  of this sample. Moreover, both treatments are responsible for a decrease in  $T_g$  values, more pronounced for the sample incubated in ethanol solution, as already observed for the PTF homopolymer. Therefore, the glass transition temperature gets very close to the testing temperature, allowing the macromolecular chains to acquire greater mobility and rearranging themselves into an ordered crystalline structure. The same trend was observed for the sample containing 15% of the TSeb co-unit, while the sample containing 25% of the TSeb co-unit showed a different behavior. As this material was rubbery and semicrystalline before the stress treatments, after food simulant contact only a slight decrease in  $T_g$  values was observed, together with a shift towards slightly higher temperatures of the lower melting peak, as a result of annealing at 40 °C. However,

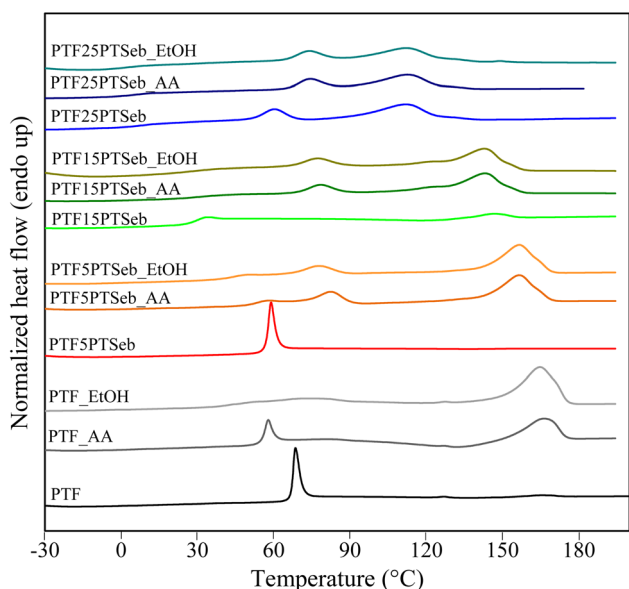


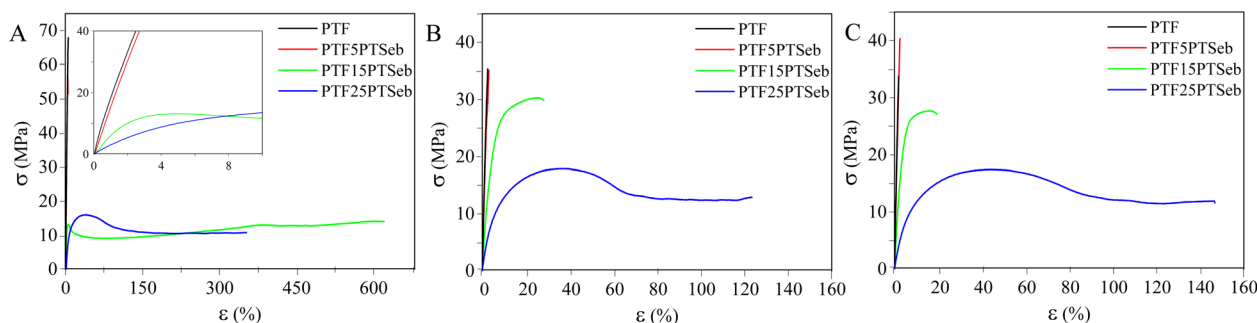
**Fig. 7** DSC heating scans at a rate of 20 °C min<sup>-1</sup> for PTF and PTFcoPTSeb copolymers before and after food simulant contact.



**Table 6** Tensile properties of PTF and PTFcoPTSeb copolymers films before and after food simulant contact (ethanol 10% v/v; acetic acid 3% w/v)<sup>a</sup>

Sample	Young's modulus ( $E$ , MPa)			Stress at break ( $\sigma_B$ , MPa)			Elongation at break ( $\epsilon_B$ , %)		
	Control	EtOH	Acetic acid	Control	EtOH	Acetic acid	Control	EtOH	Acetic acid
PTF	2050 ± 180 <sup>d</sup>	1730 ± 105 <sup>d</sup>	2080 ± 60 <sup>d</sup>	64 ± 3 <sup>d</sup>	35 ± 1 <sup>c</sup>	32 ± 2 <sup>b</sup>	5 ± 1 <sup>a</sup>	3 ± 1 <sup>a</sup>	2 ± 1 <sup>a</sup>
PTF5PTSeb	1830 ± 160 <sup>c</sup>	1560 ± 32 <sup>c</sup>	1900 ± 90 <sup>c</sup>	56 ± 5 <sup>c</sup>	39 ± 4 <sup>c</sup>	39 ± 1 <sup>c</sup>	5 ± 1 <sup>a</sup>	4 ± 1 <sup>a</sup>	3 ± 1 <sup>a</sup>
PTF15PTSeb	540 ± 90 <sup>b</sup>	662 ± 96 <sup>b</sup>	916 ± 80 <sup>b</sup>	15 ± 1 <sup>b</sup>	27 ± 2 <sup>b</sup>	32 ± 2 <sup>b</sup>	527 ± 90 <sup>c</sup>	29 ± 5 <sup>b</sup>	19 ± 2 <sup>b</sup>
PTF25PTSeb	280 ± 30 <sup>a</sup>	232 ± 23 <sup>a</sup>	223 ± 15 <sup>a</sup>	12 ± 1 <sup>a</sup>	11 ± 1 <sup>a</sup>	13 ± 1 <sup>a</sup>	300 ± 50 <sup>b</sup>	115 ± 10 <sup>c</sup>	137 ± 12 <sup>c</sup>

<sup>a</sup> Different lowercase letters within the same column indicate statistically significant differences between samples ( $p < 0.05$ ), based on ANOVA followed by Tukey's *post hoc* test.

**Fig. 8** Stress–strain curves of PTF and PTFcoPTSeb copolymers films before (A) and after stress treatment with ethanol 10% v/v food simulant (B) and acetic acid 3% w/v food simulant (C).

the overall melting enthalpy remained almost unchanged compared to the untreated sample, indicating that the testing conditions did not considerably alter the crystalline phase of this sample.

**3.4 Mechanical performances after stress treatments.** Mechanical tensile tests were recorded for each sample, at room temperature, in the form of compression moulded films, to investigate the change in the stress–strain behavior after food simulant contact. Young's modulus ( $E$ , MPa), stress at break ( $\sigma_B$ , MPa) and elongation at break ( $\epsilon_B$ , %) were collected and are summarized in Table 6, while Fig. 8 shows representative stress–strain curves of PTF and PTFcoPTSeb copolymers before and after stress treatment.

As to the untreated samples, PTF and PTF5PTSeb are the most brittle films, with the highest  $E$  and  $\sigma_B$ , and the lowest  $\epsilon_B$  value, not exceeding 5%, due to their glassy state at room temperature (Table 4). Conversely, PTF15PTSeb was found to be the best performing sample from a mechanical point of view, being the most ductile, with an elongation at break greater than 500%, associated with high chain flexibility ( $T_g$  very close to room temperature) conferred by aliphatic TSeb co-units. The PTF25PTSeb sample, instead, showed an intermediate mechanical behavior, with an elongation at break of 300%. This result is due to its rubbery ( $T_{\text{test}} = T_{\text{room}} > T_g$ ) but semi-crystalline state. Indeed, the highest percentage of TSeb units allows the development of a certain amount of the crystalline phase (Fig. 7), thus reducing the polymer flexibility. All these results are in agreement with data reported in the literature.<sup>21</sup>

After treatment with food simulant liquids, the samples underwent some changes in their mechanical properties. In particular, PTF and PTF5PTSeb samples show a reduction in breaking strength, due to the action of the simulant liquids. PTF treated with acetic acid shows a similar rigidity compared to the control, in agreement with DSC results (Fig. 7), while the sample treated with ethanol is characterized by slightly lower  $E$  values, despite the development of a consistent amount of the crystalline phase. As a result, it is reasonable that the flexibility due to the plasticizing effect imparted by this food simulant liquid prevailed over the increase in rigidity due to the development of crystallinity. As to the elongation at break values, they remained practically constant. In the case of PTF5PTSeb samples, the same trend observed for PTF can be noticed for all the mechanical parameters. In detail, a more pronounced decrease in the  $E$  value can be observed for the sample treated with ethanol compared to the one treated with acetic acid, although they both developed the same amount of the crystalline phase. Once again, it can be hypothesized that the higher plasticizing effect caused by ethanol can lead to a lower value of elastic modulus. The PTF25PTSeb samples show more or less the same behavior, except for the elongation at break that was halved. On the other hand, the copolymer PTF15PTSeb showed remarkably different behavior: in contact with simulant liquids the samples significantly increased their values of Young's modulus and stress at break, while the elongation at break decreased, from about 500% to around 115–137% in line with the increase in crystallinity (Table 4), more pronounced in the case of acetic acid.<sup>35,68,69</sup>



**Table 7** Lightness coefficient ( $L^*$ ),  $a^*$  and  $b^*$ , total color difference ( $\Delta E$ ),  $C^*$  and  $h_{ab}$  of PTF and PTFPTSeb copolymer films, before and after stress treatment<sup>a</sup>

Sample	$L^*$	$a^*$	$b^*$	$\Delta E$	$C^*$	$h_{ab}$
White standard	66.50 ± 0.01	-0.75 ± 0.00	1.35 ± 0.01	—	1.54	119
PTF	18.08 ± 0.13 <sup>a</sup>	-0.10 ± 0.01 <sup>g</sup>	-0.63 ± 0.08 <sup>c</sup>	48.47	0.64	99
PTF-ethanol	38.94 ± 0.04 <sup>g</sup>	-1.51 ± 0.00 <sup>d</sup>	-0.25 ± 0.02 <sup>fg</sup>	27.62	1.53	171
PTF-acetic acid	43.74 ± 0.40 <sup>h</sup>	-1.83 ± 0.08 <sup>cd</sup>	-0.15 ± 0.04 <sup>g</sup>	22.84	1.84	175
PTF5PTSeb	17.58 ± 0.58 <sup>a</sup>	-0.15 ± 0.01 <sup>g</sup>	-0.41 ± 0.01 <sup>f</sup>	49.35	0.44	110
PTF5PTSeb-ethanol	25.84 ± 0.63 <sup>c</sup>	-1.84 ± 0.06 <sup>cd</sup>	-2.11 ± 0.15 <sup>d</sup>	40.83	2.80	131
PTF5PTSeb-acetic acid	31.36 ± 0.11 <sup>e</sup>	-2.00 ± 0.02 <sup>c</sup>	-2.72 ± 0.09 <sup>ab</sup>	35.40	3.38	126
PTF15PTSeb	19.93 ± 0.37 <sup>b</sup>	-0.15 ± 0.02 <sup>g</sup>	-0.68 ± 0.11 <sup>e</sup>	46.62	0.70	102
PTF15PTSeb-ethanol	30.76 ± 0.16 <sup>c</sup>	-2.21 ± 0.02 <sup>b</sup>	-2.64 ± 0.01 <sup>b</sup>	36.00	3.44	130
PTF15PTSeb-acetic acid	36.30 ± 0.35 <sup>f</sup>	-2.81 ± 0.11 <sup>a</sup>	-3.07 ± 0.07 <sup>a</sup>	30.59	4.16	132
PTF25PTSeb	20.55 ± 0.39 <sup>b</sup>	-0.25 ± 0.00 <sup>fg</sup>	-2.47 ± 0.14 <sup>c</sup>	46.12	2.48	96
PTF25PTSeb-ethanol	25.37 ± 0.05 <sup>c</sup>	-0.87 ± 0.01 <sup>f</sup>	-2.39 ± 0.02 <sup>c</sup>	41.30	2.54	110
PTF25PTSeb-acetic acid	28.50 ± 0.08 <sup>d</sup>	-1.04 ± 0.01 <sup>e</sup>	-2.47 ± 0.08 <sup>bc</sup>	38.20	2.68	113

<sup>a</sup>  $h_{ab} = 0^\circ$ , red–purple;  $h_{ab} = 90^\circ$ , yellow;  $h_{ab} = 180^\circ$ , green;  $h_{ab} = 270^\circ$ , blue; different lowercase letters within the same column indicate statistically significant differences between samples ( $p < 0.05$ ), based on ANOVA, followed by Tukey's *post hoc* test, for the directly measured chromaticity coordinates  $L^*$ ,  $a^*$  and  $b^*$ .

**3.5 Color evaluation.** Transparency and color of the film are very important parameters when it is going to be commercialized. They obviously allow evaluation of the contained object, not only from the qualitative point of view but also from that of integrity. In particular, if it contains food, the color associated with the quantity of natural pigments present has always been considered one of the key parameters to evaluate the quality and flavor of the food, especially from the consumer's point of view. The packaging must therefore not influence, or do so in a very limited way, the color of the product it contains, so as not to alter its visual characteristics. In Table 7 the values recorded on the PTF and PTFPTSeb copolymer films are reported, before and after treatments.

Based on the literature, color measurements are performed in accordance with ASTM E308, using the CIE Lab color scale.<sup>42,70,71</sup> In particular, the lightness coefficient ( $L^*$ ) varies from black (0) to white (100). For any  $L^*$  value, the coordinates  $a^*$  and  $b^*$  place the color on a rectangular coordinate grid perpendicular to the  $L^*$  axis. At the origin ( $a^* = 0$  and  $b^* = 0$ ) the color is achromatic (defined as gray). Moving on the horizontal axis, a positive  $a^*$  value indicates a red–violet shade, and a negative  $a^*$  value indicates a green shade. Moving on the vertical axis, a positive  $b^*$  value indicates a yellow shade, and a negative  $b^*$  value indicates a blue shade.<sup>70</sup> The films under analysis showed an  $L^*$  closer to black, highlighting their transparency, while the values recorded for  $a^*$  and  $b^*$  indicated a weak tendency towards a yellowish color ( $h_{ab}$  over  $90^\circ$ ). Chromaticity ( $C^*$ ) is an important quality of color, as it determines both the saturation and the intensity of the color itself. A very low  $C^*$  was recorded, which means low color saturation and consequently good transparency of the film, although some differences were recorded relating to the composition of the copolymer and food simulant liquids. In particular, the copolymer containing the highest percentage of TSeb units (25%) showed a greater, albeit slight, color saturation (higher  $C^*$ ), in accordance with the highest crystallinity percentage. After

treatment with the simulant liquids, the values underwent a variation, especially in contact with the acetic acid solution, thus showing a greater interaction with this environment. An increase in the  $L^*$  value showed a decrease in translucency, with a greater tendency towards green (the  $a^*$  value moves away from zero towards a green shade) and towards blue (the  $b^*$  value becomes more negative towards a blue shade). A  $\Delta E$  value far from zero shows a low tendency of the films to whitening, even if this value decreases with the treatments undergone, compared to the untreated material. From the collected data, it can be concluded that contact with the two liquids simulating different types of food gives rise to a different appearance of the films, with consequent different percentages of crystallinity, which is the main physical parameter that influences the color behavior. In general, however, the samples showed excellent color/transparency stability. The absence of significant variations in optical properties (color and transparency), together with the stability of thermal and mechanical behavior, suggests that no detectable changes occurred at the macroscopic level after exposure to food simulants.

## 4 Conclusions

In this work, we successfully studied bio-derived aliphatic/aromatic random copolymers of poly(trimethylene 2,5-furandicarboxylate-*co*-trimethylene sebacate) (PTF-*co*-PTSeb) with the aim of evaluating their gas barrier performance under real-world application conditions.

The results demonstrated that copolymer composition plays a key role in determining the balance between stiffness, flexibility, and gas permeability. Specifically, the copolymer containing 15 mol% PTSeb exhibited the most favorable barrier performance under dry conditions, attributable to enhanced intermolecular interactions and dense amorphous packing. This study expands on previous research by moving from intrinsic material characterization to a systematic evaluation of performance under realistic conditions, including temperature



variations, high relative humidity, and exposure to food simulants. These conditions significantly influenced gas transport behavior, highlighting both the potential and limitations of these materials in practical applications.

Overall, the copolymers showed good stability after exposure to food simulants, with no significant changes in thermal, mechanical, and optical properties. These results suggest that no obvious macroscopic degradation occurred under the conditions studied. From an application perspective, the materials appear particularly suitable for dry or low-humidity food packaging, where high gas barrier properties are required. However, sensitivity to high humidity represents a limitation that must be carefully considered for applications in high-humidity or tropical environments.

Although the materials are entirely bio-based, their environmental benefits cannot be assumed *a priori* and depend on end-of-life scenarios. Further studies are needed to evaluate biodegradability, compostability under standardized conditions, and overall environmental impact through a life cycle assessment. Overall, this work provides a more application-oriented understanding of PTF-based copolymers and supports their potential as tunable materials for sustainable food packaging, clearly identifying the key parameters governing their performance.

## Author contributions

Conceptualization: V. S., G. G., A. S., and N. L.; data curation: V. S., G. G., and A. Z.; formal analysis: V. S., G. G., and A. Z.; funding acquisition: V. S., G. G., N. L., and A. S.; investigation: V. S., G. G., and A. Z.; methodology: V. S., G. G., and A. Z.; supervision and validation: V. S., A. S., and N. L.; writing original draft: V. S., and G. G.; writing – review & editing: V. S., G. G., and N. L.

## Conflicts of interest

Authors declare no conflicts of interest.

## Data availability

The datasets obtained during the current study are available from the corresponding author upon reasonable request.

## Acknowledgements

This research was funded by the Agritech National Research Center and received funding from the European Union Next-GenerationEU (PIANO NAZIONALE DI RIPRESA E RESILIENZA (PNRR)) (MISSIONE 4 COMPONENTE 2, INVESTIMENTO 1.4-D. D. 1032 17/06/2022, CN00000022). This manuscript reflects only the authors' views and opinions; neither the European Union nor the European Commission can be considered responsible for them.

## References

- 1 Plastics Europe, *Plastics – the Fast Facts*, 2025, <https://plasticseurope.org/knowledge-hub/plastics-the-fast-facts-2025/>.
- 2 M. Manfroni, A. Coatti, M. Soccio, V. Siracusa, E. Boanini, E. Salatelli and N. Lotti, *Eur. Polym. J.*, 2025, **225**, 1113728, DOI: [10.1016/j.eurpolymj.2025.1113728](https://doi.org/10.1016/j.eurpolymj.2025.1113728).
- 3 H. Ritchie, V. Samborska and M. Roser, “Plastic Pollution” Published online at OurWorldinData.org, 2023, retrieved from: <https://ourworldindata.org/plastic-pollution>.
- 4 Single-Use Plastics, *A Roadmap for Sustainability*, United Nations Environment Programme, 2018.
- 5 S. RameshKumar, P. Shaiju and K. E. O'Connor, *Curr. Opin. Green Sustainable Chem.*, 2020, **21**, 75–81, DOI: [10.1016/j.cogsc.2019.12.005](https://doi.org/10.1016/j.cogsc.2019.12.005).
- 6 M. S. Kim, H. Chang, L. Zheng, Q. Yan, B. F. Pflieger, J. Klier, K. Nelson, E. L. W. Majumder and G. W. Huber, *Chem. Rev.*, 2023, **123**, 9915–9939, DOI: [10.1021/acs.chemrev.2c00876](https://doi.org/10.1021/acs.chemrev.2c00876).
- 7 K. Y. Perera, A. K. Jaiswal and S. Jaiswal, *Foods*, 2023, **12**, DOI: [10.3390/foods12122422](https://doi.org/10.3390/foods12122422).
- 8 N. Peelman, P. Ragaert, B. De Meulenaer, D. Adons, R. Peeters, L. Cardon, F. Van Impe and F. Devlieghere, *Trends Food Sci. Technol.*, 2013, **32**, 128–141, DOI: [10.1016/j.tifs.2013.06.003](https://doi.org/10.1016/j.tifs.2013.06.003).
- 9 *Global Production capacities of bioplastics 2023–2028*, 2023, <https://www.european-bioplastics.org/news/publica->, online resource.
- 10 G. L. Robertson, Chapter 2: Structure and Related Properties of Plastic Polymers, in *Food Packaging—Principles and Practice*, 3rd edn, Taylor & Francis Group, CRC Press, Boca Raton, FL, USA, 2013, pp. 91–130, ISBN 978-1-4398-6242-1.
- 11 B. Program, T. Werpy and G. Petersen, Top Value Added Chemicals from Biomass Volume I-Results of Screening for Potential Candidates from Sugars and Synthesis Gas Produced by the Staff at Pacific Northwest National Laboratory (PNNL) National Renewable Energy Laboratory (NREL) Office of Biomass Program (EERE) For the Office of the Energy Efficiency and Renewable Energy, 2024, <https://www.osti.gov/bridge>.
- 12 S. Pandey, M. J. Dumont, V. Orsat and D. Rodrigue, *Eur. Polym. J.*, 2021, **160**, 110778, DOI: [10.1016/j.eurpolymj.2021.110778](https://doi.org/10.1016/j.eurpolymj.2021.110778).
- 13 K. Nasr, A. Favrelle-Huret, R. Mincheva, G. Stoclet, M. Bria, J. M. Raquez and P. Zinck, *ACS Appl. Polym. Mater.*, 2022, **4**, 1387–1400, DOI: [10.1021/acsapm.1c01777](https://doi.org/10.1021/acsapm.1c01777).
- 14 E. Bianchi, L. Papadopoulos, M. Soccio, V. Siracusa, M. Gazzano, T. Robert, D. N. Bikiaris and N. Lotti, *Polym. Degrad. Stab.*, 2024, **230**, 111049, DOI: [10.1016/j.polymdegradstab.2024.111049](https://doi.org/10.1016/j.polymdegradstab.2024.111049).
- 15 E. Bianchi, M. Soccio, V. Siracusa, M. Gazzano, S. Thiyagarajan and N. Lotti, *React. Funct. Polym.*, 2024, **203**, 106010, DOI: [10.1021/acssuschemeng.1c04104.811](https://doi.org/10.1021/acssuschemeng.1c04104.811).
- 16 A. F. Sousa, R. Patrício, Z. Terzopoulou, D. N. Bikiaris, T. Stern, J. Wenger, K. Loos, N. Lotti, V. Siracusa, A. Szymczyk, S. Paszkiewicz, K. S. Triantafyllidis,



- A. Zamboulis, M. S. Nikolic, P. Spasojevic, S. Thiyagarajan, D. S. van Es and N. Guigo, *Green Chem.*, 2021, **23**, 8795–8820, DOI: [10.1039/D1GC02082J](https://doi.org/10.1039/D1GC02082J).
- 17 J. Zhang, Y. Liu, Z. Qi, L. He and L. Peng, *BioResources*, 2020, **15**, 4502–4527, DOI: [10.15376/biores.15.2.4502-4527](https://doi.org/10.15376/biores.15.2.4502-4527).
- 18 X. Fei, J. Wang, J. Wang, J. Zhu, X. Wang and X. Liu, *ACS Sustain. Chem. Eng.*, 2020, **8**, 8471–8485, DOI: [10.1021/acssuschemeng.0c01862](https://doi.org/10.1021/acssuschemeng.0c01862).
- 19 A. Zubkiewicz, A. Szymczyk, J. Dryzek, Z. Rozwadowski, R. J. Sablong, M. Soccio, G. Guidotti, V. Siracusa and N. Lotti, *Eur. Polym. J.*, 2025, **22316**, 113673, DOI: [10.1016/j.eurpolymj.2024.113673](https://doi.org/10.1016/j.eurpolymj.2024.113673).
- 20 V. Tsanaktis, G. Z. Papageorgiou and D. N. Bikiaris, *J. Polym. Sci., Part A: Polym. Chem.*, 2015, **53**, 2617–2632, DOI: [10.1002/pola.27730](https://doi.org/10.1002/pola.27730).
- 21 A. Zubkiewicz, A. Szymczyka, R. J. Sablong, M. Soccio, G. Guidotti, V. Siracusa and N. Lotti, *Polym. Degrad. Stab.*, 2022, **195**, 109800, DOI: [10.1016/j.polymdegradstab.2021.109800](https://doi.org/10.1016/j.polymdegradstab.2021.109800).
- 22 M. Kwiatkowska, I. Kowalczyk, K. Kwiatkowski, A. Szymczyk and Z. Roslaniec, *Polymers*, 2016, **99**, 503–512, DOI: [10.1016/j.polymer.2016.07.060](https://doi.org/10.1016/j.polymer.2016.07.060).
- 23 H. Hu, R. Zhang, J. Wang, W. Bin Ying and J. Zhu, *Eur. Polym. J.*, 2018, **102**, 101–110, DOI: [10.1016/j.eurpolymj.2018.03.009](https://doi.org/10.1016/j.eurpolymj.2018.03.009).
- 24 Z. Terzopoulou, L. Papadopoulos, A. Zamboulis, D. G. Papageorgiou, G. Z. Papa-georgiou and D. N. Bikiaris, *Polymers*, 2020, **12**(6), 1209, DOI: [10.3390/POLYM12061209](https://doi.org/10.3390/POLYM12061209).
- 25 G. Guidotti, L. Genovese, M. Soccio, M. Gigli, A. Munari, V. Siracusa and N. Lotti, *Int. J. Mol. Sci.*, 2019, **20**, 2187, DOI: [10.3390/ijms20092187](https://doi.org/10.3390/ijms20092187).
- 26 D. Perin, D. Rigotti, G. Fredi, G. Z. Papageorgiou, D. N. Bikiaris and A. Dorigato, *J. Polym. Environ.*, 2021, **29**, 3948–3963, DOI: [10.1007/s10924-021-02161-y](https://doi.org/10.1007/s10924-021-02161-y).
- 27 N. Pouloupoulou, N. Kasmi, M. Siampani, Z. N. Terzopoulou, D. N. Bikiaris, D. S. Achilias, D. G. Papageorgiou and G. Z. Papageorgiou, *Polymers*, 2019, **11**(3), 556, DOI: [10.3390/polym11030556](https://doi.org/10.3390/polym11030556).
- 28 M. Jiang, Q. Liu, Q. Zhang, C. Ye and G. Zhou, A series of furan-aromatic polyesters synthesized *via* direct esterification method based on renewable resources, *J. Polym. Sci., Part A: Polym. Chem.*, 2012, **50**, 1026–1036, DOI: [10.1002/pola.25859](https://doi.org/10.1002/pola.25859).
- 29 A. A. Hunashyal, S. P. Masti, L. K. Kurabetta, M. N. Gunaki, J. P. Pinto, P. Priyadarshini, S. G. Havanur, B. A. Sheeparamatti, P. Baburao and R. B. Chougale, *Sustainable Food Technol.*, 2026, DOI: [10.1039/d5fb00817d](https://doi.org/10.1039/d5fb00817d).
- 30 J. P. Pinto, M. B. Megalamani, A. A. Hunashyal, O. J. D'souza, S. T. Nandibewoor, S. P. Masti and R. B. Chougale, *RSC Pharm.*, 2026, **3**, 150, DOI: [10.1039/d5pm00172b](https://doi.org/10.1039/d5pm00172b).
- 31 A. A. Hunashyal, S. P. Masti, L. K. Kurabetta, M. N. Gunaki, S. Madihalli, J. P. Pinto, M. B. Megalamani, B. Thokchom, R. B. Yarajarla and R. B. Chougale, *Sustainable Food Technol.*, 2025, **3**, 2088, DOI: [10.1039/d5fb00358j](https://doi.org/10.1039/d5fb00358j).
- 32 S. Valentina and I. Carlo, *Polym. Test.*, 2017, **59**, 277–289, DOI: [10.1016/j.polymertesting.2017.01.011](https://doi.org/10.1016/j.polymertesting.2017.01.011).
- 33 *Gas Permeability Testing Manual*, Brugger Feinmechanik GmbH, Registergericht Munchen, Germany, 2008, [https://brugger-feinmechanik.com/wp-content/uploads/datasheets/GDP-C\\_Factsheet\\_EN.pdf](https://brugger-feinmechanik.com/wp-content/uploads/datasheets/GDP-C_Factsheet_EN.pdf).
- 34 V. Siracusa, *Int. J. Polym. Sci.*, 2012, **1**, 1–11, DOI: [10.1155/2012/302029](https://doi.org/10.1155/2012/302029).
- 35 V. Siracusa, M. Dalla Rosa and A. L. Iordanskii, *Materials*, 2017, **10**(8), 850, DOI: [10.3390/ma10080850](https://doi.org/10.3390/ma10080850).
- 36 NIST-National Institution of Standards and Technology, *Guide for the Use of the International System of Units (SI); Special Publication 811*, ed Thompson, A. and Taylor, B. N., U.S. Department of Commerce, Washington, DC, USA, 2008, <https://www.nist.gov/pml/special-publication-811>.
- 37 European Union (EU), Regulation No. 10/2011 on Plastic Materials and Articles Intended to Come into Contact with Food, available online: <https://eur-lex.europa.eu/legal-content/EN/ALL/?uri=CELEX3A32011R0010>.
- 38 Standard Practice for Computing the Colors of Objects by Using the CIE System, <https://store.astm.org/e0308-22.html>.
- 39 V. Glicerina, F. Balestra, M. Dalla Rosa, B. Berghensthal, E. Tornberg and S. Romani, *J. Food Sci.*, 2014, **79**(7), E1359–E1365, DOI: [10.1111/1750-3841.12508](https://doi.org/10.1111/1750-3841.12508).
- 40 S. Galus and A. Lenart, *J. Food Eng.*, 2013, **115**(4), 459–465, DOI: [10.1016/j.jfoodeng.2012.03.006](https://doi.org/10.1016/j.jfoodeng.2012.03.006).
- 41 K. Syahidad, S. Rosnah, M. A. Noranizan, O. Zaulia and A. Anvarjon, *Int. J. Res.* 2015, **22**(2), 753–760, <https://scispace.com/pdf/quality-changes-of-fresh-cut-cantaloupe-cucumis-melo-l-var-2amtfc6ns8.pdf>.
- 42 V. Siracusa, L. Genovese, C. Ingrao, A. Munari and N. Lotti, *Polymers*, 2018, **10**(5), 502, DOI: [10.3390/polym10050502](https://doi.org/10.3390/polym10050502).
- 43 G. L. Robertson, Chapter 4: Optical, Mechanical and Barrier Properties of Thermoplastic Polymers, in *Food Packaging—Principles and Practice*, 3rd edn, Taylor & Francis Group, CRC Press, Boca Raton, FL, USA, 2013, pp. 91–130, ISBN 978-1-4398-6242-1.
- 44 L. Genovese, N. Lotti, M. Gazzano, V. Siracusa, M. Dalla Rosa and A. Munari, *Polym. Degrad. Stab.*, 2016, **132**, 191–201, DOI: [10.1016/j.polymdegradstab.2016.02.022](https://doi.org/10.1016/j.polymdegradstab.2016.02.022).
- 45 Y. S. Hu, V. Prattipati, S. Mehta, D. A. Schiraldi, A. Hiltner and E. Baer, *Polymers*, 2005, **46**(8), 2685–2698, DOI: [10.1016/j.polymer.2005.01.056](https://doi.org/10.1016/j.polymer.2005.01.056).
- 46 M. Shmid, W. Zillinger, K. Muller and S. Sangerlaub, *Food Packag. Shelf Life*, 2015, **6**, 21–29, DOI: [10.1016/j.fpsl.2015.08.002](https://doi.org/10.1016/j.fpsl.2015.08.002).
- 47 L. Genovese, N. Lotti, V. Siracusa and A. Munari, *Materials*, 2017, **10**(9), 1028, DOI: [10.3390/ma10091028](https://doi.org/10.3390/ma10091028).
- 48 B. A. Sheeparamatti, P. Baburao, P. Priyadarshini, S. G. Havanur, R. B. Chougale, M. N. Gunaki, A. A. Hunashyal, S. P. Masti, N. P. Dalbanjan and S. K. Praveen Kumar, *RSC Appl. Polym.*, 2026, **4**, 767, DOI: [10.1039/d5lp00339c](https://doi.org/10.1039/d5lp00339c).
- 49 A. A. Hunashyal, S. P. Masti, M. P. Eelager, O. J. D'souza, L. K. Kurabetta, M. N. Gunaki, S. Madihalli, J. P. Pinto, M. B. Megalamani and R. B. Chougale, *Next Nanotechnol.*, 2025, **8**, 100292, DOI: [10.1016/j.nxnano.2025.100292](https://doi.org/10.1016/j.nxnano.2025.100292).



- 50 P. Atkins and L. Jones, *Chemical Principles: the Quest for Insight*, 5th edn; Freeman WH & Co., New York, NY, USA, 2012.
- 51 J. A. de Sales, P. S. O. Patricio, J. C. Machado, G. G. Silva and D. Windmoller, *J. Membr. Sci.*, 2008, **310**(1–2), 129–140, DOI: [10.1016/J.memsci.2007.10.045](https://doi.org/10.1016/J.memsci.2007.10.045).
- 52 E. Lasseguette, R. Malpass-Evans, M. Carta, N. B. McKeown and M. C. Ferrari, *Membranes*, 2018, **8**(4), 132, DOI: [10.3390/membranes8040132](https://doi.org/10.3390/membranes8040132).
- 53 T. C. Merkel, V. Bondar, K. Nagai, B. D. Freeman and Y. P. Yampolskii, *Macromolecules*, 1999, **32**(25), 8427–8440, DOI: [10.1021/ma990685r](https://doi.org/10.1021/ma990685r).
- 54 A. Yu. Alentiev, V. P. Shantarovich, T. C. Merkel, V. I. Bondar, B. D. Freeman and Yu. P. Yampolskii, *Macromolecules*, 2002, **35**(25), 9513–9522, DOI: [10.1021/ma020494f](https://doi.org/10.1021/ma020494f).
- 55 T. Komatsuka and K. Nagai, *Polym. J.*, 2009, **41**, 455–458, DOI: [10.1295/polymj.PJ2008266](https://doi.org/10.1295/polymj.PJ2008266).
- 56 T. Masuda, Y. Iguchi, B.-Z. Tang and T. Higashimura, *Polymers*, 1988, **29**(11), 2041–2049, DOI: [10.1016/0032-3861\(88\)90178-4](https://doi.org/10.1016/0032-3861(88)90178-4).
- 57 M. C. Celina and A. Quintana, *Polymers*, 2018, **150**, 326–342, DOI: [10.1016/J.polymer.2018.06.047](https://doi.org/10.1016/J.polymer.2018.06.047).
- 58 R. A. Auras, B. Harte, S. Selke and R. Hernandez, *J. Plast. Film Sheeting*, 2003, **19**(2), 123–135, DOI: [10.1177/8756087903039702](https://doi.org/10.1177/8756087903039702).
- 59 S. W. Kim and H. M. Choi, *Korean J. Chem. Eng.*, 2016, **33**(1), 330–336, DOI: [10.1007/s11814-015-0142-7](https://doi.org/10.1007/s11814-015-0142-7).
- 60 M. S. Hedenqvist, *Barrier Packaging Materials*, 2nd edn, Elsevier, 2012, DOI: [10.1016/B978-1-4377-3455-3.00027-4](https://doi.org/10.1016/B978-1-4377-3455-3.00027-4).
- 61 G. Guidotti, M. Soccio, M. C. García-Gutiérrez, T. Ezquerro, V. Siracusa, E. Gutiérrez-Fernández, A. Munari and N. Lotti, *ACS Sustain. Chem. Eng.*, 2020, **8**, 9558–9568, DOI: [10.1021/ACSSUSCHEMENG.0C02840](https://doi.org/10.1021/ACSSUSCHEMENG.0C02840).
- 62 Y. Zhang, B.-L. Liu, L.-J. Wang, Y.-H. Deng, S.-Y. Zhou and J.-W. Feng, *Polymers*, 2019, **11**(5), 818, DOI: [10.3390/polym11050818](https://doi.org/10.3390/polym11050818).
- 63 R. A. O. Bernal, R. O. Olekhovich and M. V. Uspenskaya, *Polymers*, 2023, **15**(18), 3719, DOI: [10.3390/polym15183719](https://doi.org/10.3390/polym15183719).
- 64 M. B. Yaffe and E. J. Kramer, *J. Mater. Sci.*, 1981, **16**, 2130–2136, DOI: [10.1007/BF00542373](https://doi.org/10.1007/BF00542373).
- 65 F. Iñiguez-Franco, R. Auras, G. Burgess, D. Holmes, X. Fang, M. Rubino and H. Soto-Valdez, *Polymers*, 2016, **99**, 315–323, DOI: [10.1016/j.polym.2016.07.018](https://doi.org/10.1016/j.polym.2016.07.018).
- 66 T. Koike, Y. Muranaka, H. Shibazaki, A. Onishi and T. Maki, *Polym. Degrad. Stab.*, 2025, **241**, 111573, DOI: [10.1016/j.polymdegradstab.2025.111573](https://doi.org/10.1016/j.polymdegradstab.2025.111573).
- 67 S. Martínez-Vila, L. Riera-Malgosa, R. Prieto-Fuentes, A. Duran-Serra and F. Carrillo-Navarrete, *Sustainable Chem. Pharm.*, 2025, **43**, 101891, DOI: [10.1016/j.sco.2024.101891](https://doi.org/10.1016/j.sco.2024.101891).
- 68 J. C. Halpi and K. L. Kardos, *J. Appl. Phys.*, 1972, **43**(5), 2235–2241, DOI: [10.1063/1.1661482](https://doi.org/10.1063/1.1661482).
- 69 N. Dusunceli and O. U. Colak, *Int. J. Plast.*, 2008, **24**(7), 1224–1242, DOI: [10.1016/j.ijplas.2007.09.003](https://doi.org/10.1016/j.ijplas.2007.09.003).
- 70 R. G. McGuire, *HortScience*, 1992, **27**, 1254–1255, DOI: [10.21273/HORTSCI.27.12.1254](https://doi.org/10.21273/HORTSCI.27.12.1254).
- 71 V. Siracusa, N. Lotti, A. Munari and M. Dalla Rosa, *Polym. Degrad. Stab.*, 2015, **119**, 35–45, DOI: [10.1016/j.polymdegradstab.2015.04.026](https://doi.org/10.1016/j.polymdegradstab.2015.04.026).

